Thermodynamics of Aβ(1−40) Amyloid Fibril Elongation[†]

Brian O'Nuallain, Shankaramma Shivaprasad, Indu Kheterpal,[‡] and Ronald Wetzel*

Graduate School of Medicine, University of Tennessee, 1924 Alcoa Highway, Knoxville, Tennessee 37920

Received May 18, 2005; Revised Manuscript Received July 19, 2005

ABSTRACT: We describe herein the characterization of the equilibrium point for Aβ(1−40) amyloid fibril elongation in phosphate-buffered saline at 37 °C. Seeded fibril elongation progresses rapidly to a reproducible end point of 0.7−1.0 μM unpolymerized monomeric peptide. This remaining monomeric material is functional, since after concentration it supports fibril elongation. Incubation of fibrils in the same buffer results in dissociation to a final monomer concentration in the same range. This robust C_r value is equivalent to the Aβ(1−40) fibril dissociation constant, K_d. The fact that a similar value for K_d is obtained from a ratio of dissociation and elongation rate constants further supports the view that these values are associated with a position of dynamic equilibrium and therefore are related to free energies of amyloid fibril elongation. The C_r value reported here for wild-type Aβ(1−40) fibrils corresponds to a free energy of fibril elongation of about −9 kcal/mol, a value similar to free energies of folding for small globular proteins. Elongation and dissociation of amyloid fibrils from point mutants of Aβ(1−40) also yield C_r values, different for different mutants, that reflect stabilizing/destabilizing effects. Interestingly, assembly of Aβ(1−40) fibrils in the presence of a saturating concentration of the amyloid dye thioflavin T does not measurably affect fibril stability, in contrast to the commonly observed stabilization of globular proteins by ligand binding. The ability to quantify and compare amyloid fibril thermodynamic stabilities makes it possible to include fibrils, and potentially other aggregates, in quantitative descriptions of protein folding landscapes.

Although recent interest has brought particular attention to amyloid fibrils and amyloid-like structures, the phenomenon of non-native protein aggregation extends beyond pathology to normal biology, biotechnology, and fundamental protein folding and encompasses aggregates formed during both protein folding and unfolding, both in vivo and in vitro (*1*, *2*). Traditionally, such aggregates have been considered to form essentially irreversibly. For example, amyloid fibrils, including fibrils from the Alzheimer's plaque protein Aβ[1] (*3*), are normally referred to as being highly stable and highly insoluble. At the same time, most protein aggregates, including amyloid fibrils, are composed of unfolded or misfolded proteins held together by noncovalent interactions. If this is an accurate representation of aggregate structure, aggregates in principle should be capable of undergoing the opposite, dissociation reaction, ultimately establishing a point of dynamic equilibrium. That reversibility is normally not observed under native conditions has been attributed to kinetic barriers due perhaps to an aggregate structure featuring highly intertwined chains (*4*). Although such models may often be valid, aggregates that involve higher levels of regular structure, such as amyloid fibrils, might be expected to exhibit some degree of reversibility under assembly conditions. The ability to demonstrate and quantify the position of dynamic equilibrium implicit in such reversibility not only would be a satisfying confirmation of theory but also would allow these aggregates to be placed on a common free energy surface with the unfolded and folded states, providing a more complete thermodynamic description of the folding/misfolding energy landscape (*5*). Furthermore, the ability to assign free energy values to transformations involving the aggregated state would allow rigorous quantitation of mutational and other effects, in analogy to methods now in common practice in the analysis of reversible protein folding reactions (*6*).

Some amyloid systems have been reported previously to exhibit finite, nonzero end points. In one series of examples, Lansbury and co-workers demonstrated that amyloidogenic Aβ peptides have reproducible C_r values that can be approached both from the soluble peptide side and from the aggregate side (*7*, *8*). These results for the first time suggested that characteristic end points, that might be associated with a dynamic equilibrium, can be measured for at least some amyloid formation reactions. Since such C_r values for amyloid fibril growth and dissolution would be equivalent to the fibril dissociation equilibrium constant (*9*), these values should be convertible to free energy values that have the same utility in the analysis of fibril assembly reactions as do free energies of folding for protein folding reactions (*6*).

Despite this promise, little work has been reported on exploring the robustness of amyloid fibril assembly C_r values, the legitimacy of considering them to represent positions of dynamic equilibrium, and the limits to their determination

[†] This work was conducted with funding support through Grants R01 AG18416 (R.W.) and R01 AG18927 (R.W.) from the National Institutes of Health.

* To whom correspondence should be addressed. Phone: 865-544-9168. Fax: 865-544-9235. E-mail: rwetzel@mc.utmck.edu.

[‡] Current address: Center for BioModular Multi-Scale Systems, Louisiana State University, Baton Rouge, LA 70803.

[1] Abbreviations: Aβ, the amyloid β-peptide; ThT, thioflavin T; PBS, phosphate-buffered saline; PBSA, PBS containing 0.05% sodium azide; SPR, surface plasmon resonance.

10.1021/bi050927h CCC: $30.25
Published on Web 08/30/2005

and use. Previously, we used measured C_r values for the forward fibril elongation assay to assess the energetic effects of proline mutation in the Aβ(1−40) sequence (*10*). Here we characterize the robustness of this apparent thermodynamic end point for Aβ(1−40) and some point mutants. The results confirm that in some systems C_r values can be obtained, using analytical HPLC on unlabeled peptides, which legitimately represent the thermodynamic stability of the amyloid fibril, allowing the determination of a free energy of fibril elongation. As an example, we show that saturation of the thioflavin T binding site on Aβ fibrils does not produce a measurable stabilization of the fibril against dissociation.

MATERIALS AND METHODS

Materials and General Methods. Aβ(1−40) peptides were obtained from the Keck Biotechnology Center at Yale University. Wild-type peptide was obtained pure via the large-scale synthesis option. Point mutants were obtained impure through the small scale option and purified by reverse-phase HPLC as described (*10*). All peptides were pure by HPLC and chemically confirmed by mass spectrometry. Peptides were disaggregated as described (*11*, *12*). Analytical HPLC was performed on a Agilent 1100 system on a C3 reverse-phase Zorbax column (Agilent) developed with a gradient of acetonitrile in aqueous 0.05% trifluoroacetic acid (Pierce) as described (*13*). The eluate was monitored at 215 nm, and the integrated Aβ(1−40) peak was converted to micrograms from a standard curve calibrated from an Aβ(1−40) stock whose concentration was determined by amino acid composition analysis (*13*). Thioflavin T measurements (*14*, *15*) were performed by transferring an aliquot of the reaction mixture into a cuvette containing 10 μM ThT (Sigma) in PBS (FisherBiotech BP665-1), as described (*12*). Hydrogen−deuterium exchange experiments were performed and analyzed as described (*16*, *17*). Amyloid assembly reactions were routinely conducted in PBS buffer containing 0.05% sodium azide (PBSA).

Seed Preparations. Fibril seeds were prepared as described (*12*) by removing unreacted Aβ(1−40) from a previous elongation reaction mixture by centrifugation at 20200*g* in an Eppendorf centrifuge for 25 min at room temperature. The fibril pellet was resuspended in PBSA to generate a stock suspension that was quantified by dissolving an aliquot in aqueous formic acid, injecting onto analytical HPLC (see above), and determining the mass of Aβ in the aliquot.

Theoretical Treatment of Fibril Elongation and Dissociation Kinetics. The reaction kinetics of fibril elongation and dissociation are complex, but several reasonable approximations allow treatment of kinetic data, especially if, as done here, the focus is on seeded elongation rather than nucleation-dependent growth. Reactions studied here were seeded sufficiently strongly that spontaneous nucleation is insignificant, thus eliminating the lag phase (*12*).

The basic mechanism for fibril elongation and dissociation, via monomer addition and dissociation, that should apply under these conditions is shown in eq 1. The reaction is written as a dissociation reaction, since the major term of interest in this paper, the critical concentration C_r, is equivalent to the *dissociation* equilibrium constant K_d. This is because, at equilibrium, the molar concentration of fibrils does not change as fibrils are elongated or shortened by small additions and deletions of monomer, so that the expression for K_d reduces to the concentration of monomers at equilibrium, or C_r, as shown in eq 2. The fibril growth equilibrium constant, K_a, is then simply the reciprocal of C_r.

$$\text{Fibril}_{n+1} \underset{k_{+1}}{\overset{k_{-1}}{\rightleftharpoons}} \text{Fibril}_n + \text{Monomer} \quad (1)$$

$$K_d = [\text{fibril}_n][\text{monomer}]/[\text{fibril}_{n+1}] = [\text{monomer}] = C_r = k_{-1}/k_{+1} \quad (2)$$

If all fibrils in an amyloid population, regardless of length, elongate according to the same rate constant, then fibril elongation is governed by a second-order rate constant k_{+1} and is first order in the molar concentration of both monomers and fibril growing ends (eq 3). Correspondingly, fibril dissociation is first order in the molar concentration of fibril growing ends and is governed by the first-order rate constant k_{-1} (eq 4). Unfortunately, the average molar concentration of fibrils or elongation sites in a fibril population has not proved simple to determine (but see ref *18*). Fortunately, however, it is possible to make further simplifications in the kinetics so that this value is not required for some treatments of the data. Thus, if secondary nucleation and fragmentation (*19*) are negligible, which they appear to be in the strongly seeded reactions studied here, then the molar concentration of fibrils does not change significantly, at least in the early phase of the reaction. This assumption allows the elongation kinetics to be treated as a pseudo-first-order reaction controlled by the pseudo-first-order rate constant k_+ (eq 5), where $k_+ = k_{+1}$[fibril] (*14*). Likewise, fibril molar concentration will not change during the early stages of the fibril dissociation reaction, only beginning to decline as individual fibrils begin to disappear. This assumption allows the dissociation kinetics to be treated as a pseudo-zero-order reaction controlled by the pseudo-zero-order rate constant k_- (eq 6), where $k_- = k_{-1}$[fibril] and is equivalent to the observed dissociation rate.

$$\text{observed elongation rate} = k_{+1}[\text{fibril}][\text{monomer}] \quad (3)$$

$$\text{observed dissociation rate} = k_{-1}[\text{fibril}] \quad (4)$$

$$\text{observed elongation rate} = k_+[\text{monomer}] \quad (5)$$

$$\text{observed dissociation rate} = k_- \quad (6)$$

$$K_d = k_{-1}/k_{+1} = k_-/k_+ \quad (7)$$

One implication of this analysis is that it should be possible, in principle, to independently determine K_d from a ratio of the rate constants k_+ and k_- determined under conditions in which fibril concentrations do not change or can be interrelated (eq 7).

Analysis of Elongation Kinetics for Reactions Exhibiting a Finite Critical Concentration. The existence of a finite equilibrium position at the end of a reaction implies a significant back-reaction. There are two implications for kinetic analysis. First, the rate constant obtained is actually k_{obs}, which is the sum of the rate constants for forward and backward reactions. Second, the kinetic data reflect a reaction that is proceeding toward a finite equilibrium position, not complete and irreversible aggregation. The standard kinetic treatment for a reversible first-order (or pseudo-first-order)

reaction (*20*), where $[M_0]$ is the concentration of monomer at the start of reaction, $[M_{eq}]$ is the concentration of monomer at equilibrium (or C_r), and $[M_t]$ is the concentration of monomer at time t, is shown in eq 8. In the Results section, we use data sets consisting of HPLC sedimentation values for [Aβ(1−40)] and ThT values for [fibril] to discuss and compare various approaches for determining pseudo-first-order rate constants for fibril elongation reactions.

$$\ln\left(\frac{[M_0] - [M_{eq}]}{[M_t] - [M_{eq}]}\right) = (k_{forward} + k_{reverse})t = k_{obs}t \quad (8)$$

RESULTS

A typical fibril elongation reaction of a solution of about 30 μM disaggregated Aβ(1−40) in PBS at 37 °C, seeded with 7.2 wt % of preformed Aβ(1−40) fibrils, is shown in Figure 1a. With sufficient fibril seed, no lag phase is observed, and the reaction proceeds aggressively until it begins to slow as the amount of Aβ in the solution phase diminishes. Eventually the ThT signal reaches a maximum, plateau value. Generally such ThT plateau values are taken as indicating the point of complete conversion of monomer to fibril. When the same fibril elongation reaction of Aβ(1−40) is monitored by analytical HPLC, however, it is clear that a small amount of Aβ remains unpolymerized (Figure 1a). This residual Aβ concentration, for wild-type Aβ(1−40) under our standard conditions, invariably falls into the 0.6−1.0 μM range (Table 1, Figures 2 and 3). A previously published mean from multiple determinations is 0.86 μM (*10*), corresponding to a free energy of Aβ(1−40) fibril elongation under our standard conditions of −8.6 kcal/mol.

A trivial explanation for the existence of residual monomeric peptide at the end of the fibril reaction would be that this peptide material is chemically or conformationally altered in such a way as to render it structurally incapable of fibril growth. Thus, the chemically synthesized material we use, even though HPLC purified and exhibiting a single major parent ion in mass spectrometry, might conceivably contain low percentages of alternative structures that, if aggregation incompetent, would give rise to apparent, but artifactual, C_r values. There is no evidence, however, either from mass spectrometry or from HPLC mobility analysis (not shown) that the residual unpolymerized material in the reactions described here is chemically altered. More importantly, the residual unpolymerized material is itself clearly capable of fibril elongation. Figure 2a shows the residual monomeric Aβ(1−40) peptide isolated from a fibril elongation reaction at stasis, after concentration and seeding with fresh Aβ fibrils. The material is clearly capable of further elongation.

Another indication that the pool of monomeric Aβ at the reaction plateau represents an equilibrium pool comes from fibril dissociation reactions. Figure 2b shows the time course of monomeric Aβ(1−40) dissociation observed after a fibril elongation reaction that has reached apparent equilibrium is diluted into PBS buffer in such a way that the total Aβ concentration remains above the apparent C_r. The figure shows that monomeric Aβ dissociates from fibrils over a 24 h period until the reaction reaches a plateau concentration of 0.8−1.0 μM, the same range as for the forward fibril formation reaction (see also Table 1). This further strongly supports the contention that the residual monomeric Aβ represents a true dynamic equilibrium position of the fibril elongation reaction.

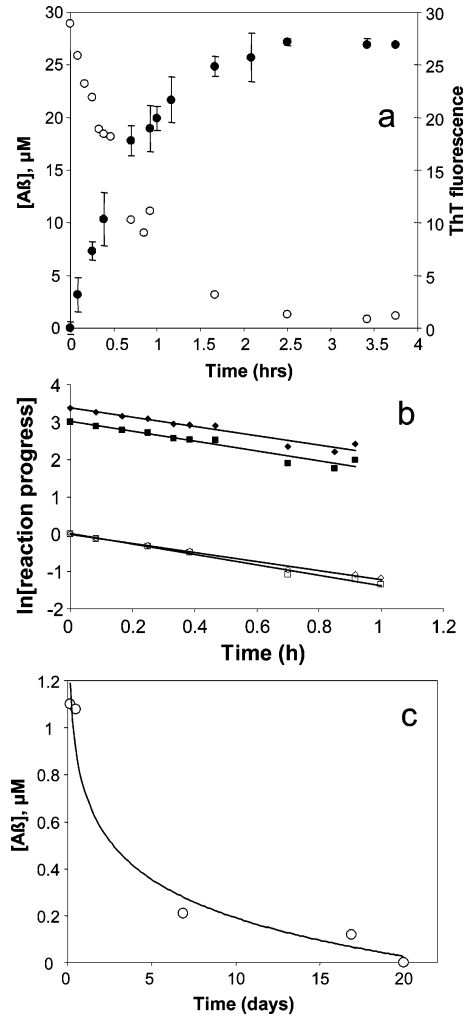

FIGURE 1: Kinetics of Aβ(1−40) amyloid fibril elongation. A freshly disaggregated solution of 29 μM peptide was seeded with 7.2 wt % of previously grown aggregates and incubated in PBSA at 37 °C. (a) Time course of increase in thioflavin T signal (●) and decrease in residual monomeric peptide determined by HPLC analysis of centrifugation supernatants (○). (b) Pseudo-first-order kinetic plots of the data in panel a plotted in various ways as described in Materials and Methods and Results. Fluorescence-based data points were multiplied times −1 so as to make them trend in parallel to the plots from monomer concentration; the plot for corrected HPLC data was shifted by +3 units to move it away from the ThT data. Data treatments as follows: unadjusted HPLC data (◆, −1.236 h^{-1}); HPLC data processed according to eq 8 (■, −1.322 h^{-1}); unadjusted ThT data (□, −1.378 h^{-1}); ThT data processed to adjust for C_r, as described in Results (◇, −1.202 h^{-1}). (c) Decay of the measured C_r value for the elongation held at 37 °C for 3 weeks. The ordinate is ln $[F_{final} - F_t]$ (□); ln $[F_{normalized} - F_t]$ (◇); ln $[A\beta(1-40)_{monomer}]$ (◆); ln{$([M_0] - [M_{eq}])/([M_t] - [M_{eq}])$} (■).

Another indication of a robust equilibrium is the ability to independently calculate the equilibrium constant from forward and reverse rates. Since fibril elongation and dissociation rates depend on the molar concentration of fibrils, as discussed in Materials and Methods, this can be done only under conditions where there is a known relationship between the fibril populations used to measure the forward and reverse reactions. Figure 3a shows the elongation kinetics of a fibril elongation reaction with 25 μM Aβ(1−

Table 1: Equilibrium Constants (μM) for Aβ(1−40) Fibril Dissociation (K_d)

Aβ(1−40) derivative	from C_r values for		elongation in the presence of ThT[a,b]
	elongation[a]	dissociation[a]	
WT	0.96 ± 0.1 (5)[c]	0.83 ± 0.1 (5)[c]	1.04
S26P	8.1	6.8	7.9
G37P	1.4	2.1	1.3

[a] Obtained as the critical concentration, C_r, determined at the fibril elongation end point (Materials and Methods). [b] Each value is an average from reactions done in the presence of 45 and 90 μM ThT (see Figure 6). [c] Standard deviations, with values in parentheses showing the number of independent determinations.

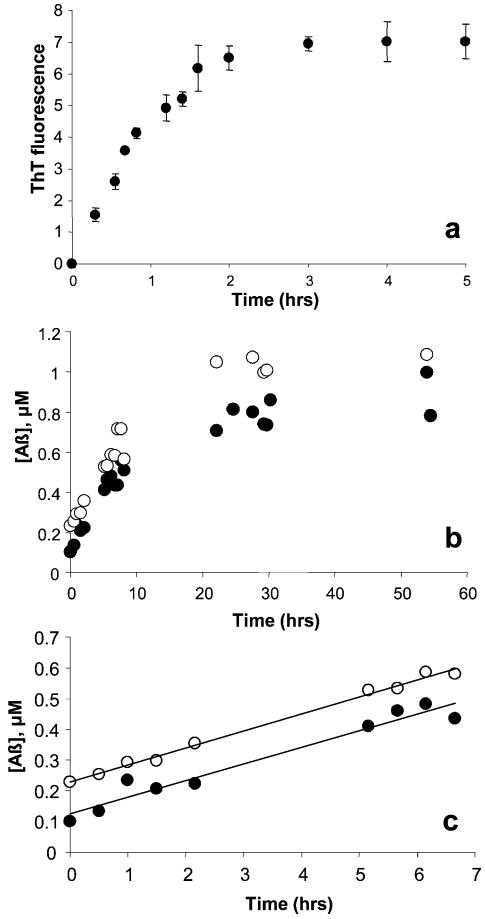

FIGURE 2: Kinetic tests of C_r robustness. (a) An equilibrium supernatant of the reaction shown in Figure 1, containing 1.1 μM Aβ(1−40), was removed from the pellet after centrifugation, concentrated to 5 μM, seeded with 31 wt % of fibril seeds, incubated at 37 °C, and monitored by the ThT reaction. (b) Aliquots of the elongation reaction shown in Figure 1c were removed at 0 days (●) and 30 days (○) and diluted in PBS to a total Aβ concentration of about 1.5 μM, and the amount of soluble Aβ present over time was determined in the HPLC sedimentation assay. (c) Data from initial time points of plots shown in panel b plotted as a zero-order reaction (Materials and Methods).

40) that was seeded with 8.4 wt % of Aβ fibrils and monitored by ThT fluorescence. Plotting ln [$F_{final} - F_t$] vs time (inset) gives a pseudo-first-order rate constant of 0.735 h^{-1}. After the reaction reached equilibrium, it was gently mixed and an aliquot removed and diluted 25-fold into fresh PBSA to give an approximate total Aβ(1−40) concentration of 1 μM. Since this is at or above the apparent C_r, we expect fibrils to dissociate, but not completely, stopping at the characteristic equilibrium position. The dissociation data

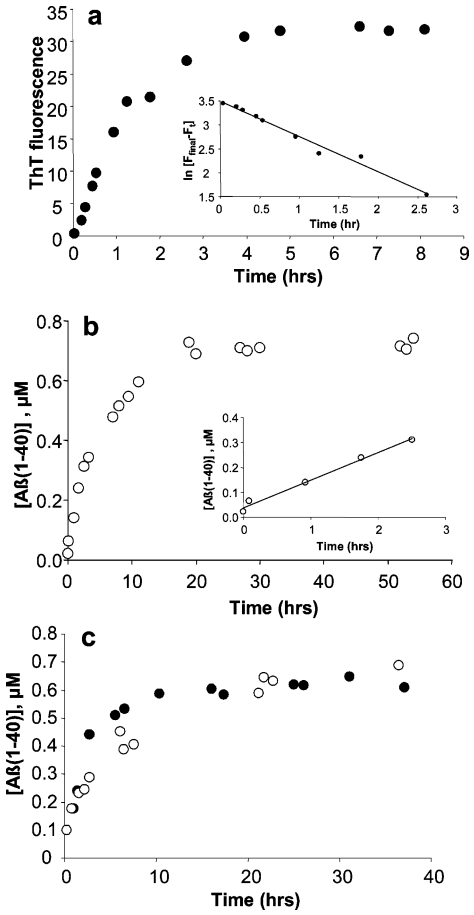

FIGURE 3: Elongation and dissociation of Aβ(1−40) fibrils. (a) 25 μM Aβ(1−40) seeded with 8.4 wt % of Aβ(1−40) fibrils and monitored by ThT fluorescence. Inset: pseudo-first-order plot of initial rate. (b) The equilibrium reaction mixture from panel a was diluted 25-fold into PBSA and incubated at 37 °C, and the Aβ released was monitored by HPLC sedimentation assay. Inset: initial rate. (c) Equal weight concentrations of two batches of Aβ(1−40) fibrils, originally grown from either 2 ng (○) or 10 ng (●) of sonicated fibril seeds (see Materials and Methods), were incubated in PBSA at 37 °C, and the concentration of soluble Aβ released over time was determined using the sedimentation HPLC assay.

(Figure 3b) show that Aβ(1−40) monomers dissociate from the fibrils over the course of 1 day, reaching a plateau value of about 0.7 μM. The early phase of the dissociation reaction, before the back- (elongation) reaction becomes significant, is linear (inset) and gives a dissociation rate of 0.111 μM/h, which is equivalent to the pseudo-zero-order rate constant for fibril dissociation under these precise conditions (Materials and Methods). Adjusting this value for the 25-fold dilution gives $k_- = 2.78$ μM/h for a concentration of fibrils identical to that used to determine the elongation rate of 0.735 h^{-1}. The K_d calculated by the k_-/k_+ ratio, then, is 2.78 μM h^{-1}/0.735 h^{-1}, or 3.8 μM. This is in reasonably good agreement with the values obtained by measuring directly the equilibrium concentration of monomeric Aβ(1−40) for forward and reverse elongation reactions (Table 1) and is thus another indication that the fibril formation reaction reaches a position of dynamic equilibrium. One possible explanation for why this calculated K_d does not more exactly match the K_d value from the measured C_r is because the rate constants used in the calculation are, of necessity, observed rate constants that are composites of the forward and reverse rate constants.

As expected, the amount of Aβ(1−40) at equilibrium does not depend on the number of growing ends in the fibril preparation, which are vastly outnumbered by the monomer concentration at equilibrium. We confirmed this by growing two batches of Aβ fibrils by seeding the same monomer concentration with either 2 or 10 ng of the same fibril seed stock. The more heavily seeded reaction is expected to yield a fibril product with a higher molar concentration of extended fibril growing ends. After both reactions went to completion, they were diluted, and fibril dissociation was monitored and analyzed as described above. As expected, initial fibril dissociation kinetics are faster for the fibrils that were seeded at a higher level (Figure 3c). Despite this difference in average fibril molecular weight, both reactions tend to the same equilibrium position, which in this experiment gave C_r values in the 0.6−0.7 μM range (Figure 3c).

A Second Phase of Fibril Stabilization. After sustaining an apparent C_r in the 1 μM range over a period of hours to days, Aβ fibril assembly reactions decay on long-term further incubation (Figure 1c) until less than 0.1 μM Aβ is detected in a high-speed centrifugation supernatant. At face value, this suggests a further assembly process that, unless understood, would threaten our ability to confidently attribute the initially observed C_r plateau to Aβ(1−40) fibril stability. Figure 2b shows, however, that fibrils incubated for 1 month at 37 °C, at which time the reaction contains no detectable level of monomeric Aβ, yield the normal expected amount of dissociated monomeric Aβ at equilibrium (i.e., the C_r) after the aged elongation reaction mixture is diluted and briefly vortexed. In fact, the reaction rates for dissociation of fresh and old fibrils are identical (Figure 2c). These data suggest that, although the low C_r of long-term incubated Aβ fibrils must reflect a true further stabilization of the amyloid, this stabilization is most likely due to some secondary self-association of the fibrils that is easily reversed by vortexing.

The suggestion that the long-term decline of the measured C_r, when a completed Aβ(1−40) elongation reaction is incubated, is due to a relatively subtle structural difference between fresh and aged fibrils is also supported by hydrogen exchange (HX) studies. HX monitored by mass spectrometry shows that aged fibrils (after mixing and buffer exchange using centrifugation and vortexing) have exactly the same complement of protective H-bonds as do fresh fibrils (Figure 4). Figure 4a shows the kinetics of exchange, corrected for side chain exchange (*16*, *17*), of fibrils isolated from elongation reactions either immediately after the ThT signal reached a plateau or 6 days after the plateau. Since the analysis times in this experiment (weeks) are long compared to the fibril ages being analyzed, we also did a comparison based only on a relatively short HX time. Figure 4b shows the mass/charge ratio after incubation for 20−22 h in D_2O for fibrils incubated in elongation buffer 0, 6, or 12 days beyond the point of ThT signal maximum. The analysis yields 10.3−11.0 deuteriums exchanged for each of these differently aged fibrils, therefore showing no detectable difference in secondary structure for fibrils recovered from short or long growth reactions. These results should be compared with side chain corrected values previously obtained for monomeric Aβ(1−40) (27.3 ± 1.1) and fibrils (11.3 ± 0.7) (*16*). Given the ability of this method to reproducibly quantify differences of one to two protected

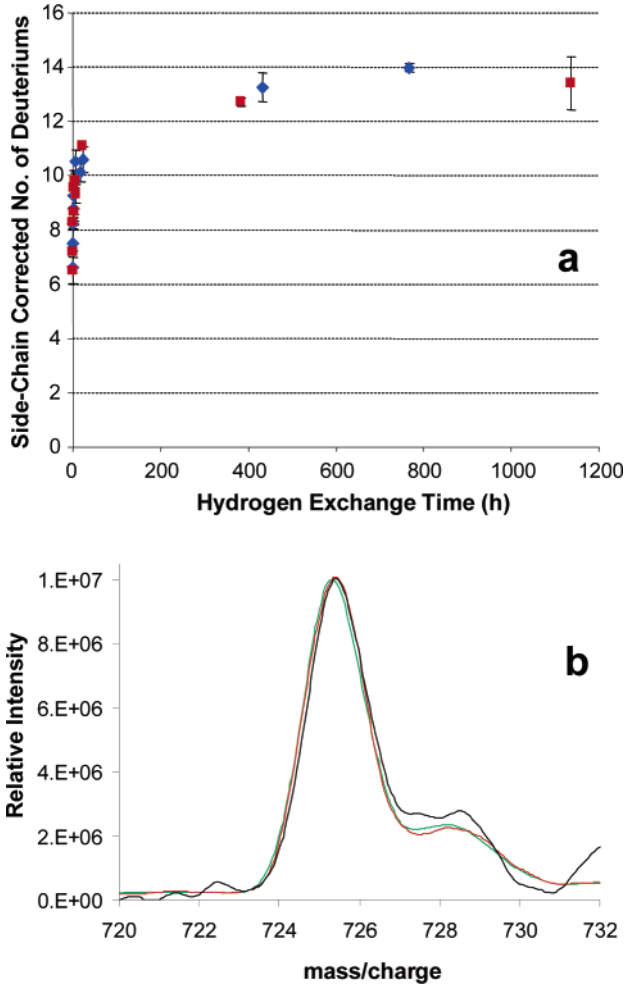

FIGURE 4: Hydrogen−deuterium exchange on fibrils aged for different times during/after elongation reactions such as those described in Figures 1 and 2. (a) Time-dependent exchange of deuterium into Aβ(1−40) in fibrils harvested from a reaction 0 (blue ◆) or 6 (red ■) days after fibril assembly was complete by the ThT reaction. (b) Single 20−22 h time point data for fibrils harvested from a reaction 0 (green), 6 (red), or 12 (black) days after fibril assembly was complete by ThT. Calculated corrected deuterium incorporation for these three fibril preparations was 10.3 (0 days), 11.0 (6 days), and 11.0 (12 days). The differences are within the error bars of the experiment.

hydrogens in amyloid fibrils from different Aβ(1−40) mutant peptides (*10*), the correspondence between fresh and aged fibrils further supports the view that they have very similar structures. While the hypothesized superaggregation of aged fibrils might possibly be mediated, at least in part, by H-bonding, this would not be expected to show up in the HX, since sample preparation included similar vortexing steps as were found, as described above, to restore the C_r to that of fresh fibrils. In any case, it is also possible that the Aβ fibrils might clump together mediated solely by hydrophobic interactions. The lack of a critical structural difference between fresh and (vortexed) aged fibrils is also supported by electron micrographs, which are also indistinguishable (data not shown).

Another possible explanation for the slow, second phase in the drop of soluble monomeric Aβ during fibril formation is that the loss is due to adsorption of monomer to the plastic surface of the reaction tubes. However, if this were to occur, we would expect additional monomers to be generated by

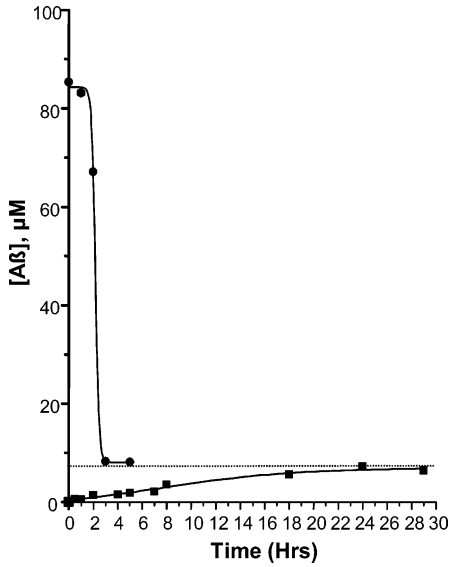

FIGURE 5: Critical concentration determination for the S26P variant of Aβ(1−40) in PBS at 37 °C. The forward fibril formation reaction (●) contained 85 μM freshly disaggregated mutant peptide and 0.1 wt % of wild-type Aβ(1−40) fibril seeds. The reverse, dissociation reaction was prepared by diluting the forward reaction in PBS to achieve a total Aβ concentration of about 10 μM (monomer equivalent) and then incubated at 37 °C (■). Significant ThT signal remained after the dissociation reaction reached equilibrium at ~30 h (not shown).

fibril dissociation to reestablish the equilibrium C_r. Fibril dissociation (Figure 2b) is much faster than the slow decrease of monomer concentration shown in Figure 1c, and once the hypothetical adsorption sites on the plastic were saturated, the equilibrium concentration of Aβ monomer would be expected to be reestablished.

Critical Concentration in the Analysis of Aβ(1−40) Mutants. One of the major potential uses of C_r-derived ΔG values is the analysis and comparison of fibril formation in response to mutagenesis. For example, we have reported C_r values and calculated apparent $\Delta\Delta G$ values for fibril stability, compared to wild type, for a series of proline substitution mutants (*10*) and for several disulfide-bonded mutants (*21*) of Aβ(1−40). Previously, these have only been determined for fibril reactions in the elongation direction. Here we asked the question of whether such C_r values for mutant fibrils are also robust, in being approachable also from the dissociation direction. Figure 5 shows the seeded fibril growth of a S26P mutant of Aβ(1−40), initiated at a starting concentration of about 85 μM. There is a rapid fibril growth phase, as evidenced by the rapid loss of Aβ from solution, reaching a plateau of about 8 μM [similar to that reported previously (*10*)] after 2−4 h of reaction. The completed fibril formation reaction was then diluted, in analogy to the reactions described above, so that both the monomer and fibril concentrations are reduced but the total Aβ concentration remains greater than 10 μM. Figure 5 shows that the S26P fibrils slowly dissociate, over a period of about 24 h, to reach an equilibrium position of monomer that is essentially the same as that obtained in the fibril growth reaction. Fibrils were still present after 24 h of dissociation, as indicated by ThT analysis (data not shown).

Table 1 shows the data from this experiment as well as similar experiments for WT and G37P Aβ(1−40). In each case, the C_r values obtained in the fibril growth and fibril dissociation directions match closely. As discussed previously, the high C_r of the S26P mutant Aβ peptide indicates a relatively unfavorable fibril formation reaction compared to that of WT, presumably because of interference of the proline with extended chain and β-sheet formation (*10*).

Table 2: Microscopic Kinetic Parameters for Aβ(1−40) Fibril Elongation[a]

	rate constant for	
mechanistic step	dissociation (s^{-1})	association
1	8.1×10^{-1}	$6.6 \times 10^{3}\ M^{-1}\ s^{-1}$
2	4.4×10^{-3}	$6.4 \times 10^{-2}\ s^{-1}$
3	4.3×10^{-4}	$4.6 \times 10^{-3}\ s^{-1}$

[a] Data from ref *22*.

Critical Concentration from SPR Experiments. The macroscopic C_r for Aβ(1−40) fibril formation of about 1 μM routinely obtained in the experiments described here is replicated in previously described SPR experiments (*22*). In the SPR experiments, Aβ(1−40) fibrils were chemically attached to the dextran layer on a Biacore chip, and then fibril formation and dissociation were studied by flowing different concentrations of rigorously disaggregated monomeric Aβ(1−40) across the immobilized fibrils. Global analysis of the data fit a three-step model for fibril growth, including an initial reversible binding step and a series of reversible conformational steps, yielding the microscopic rate constants shown in Table 2. The elongation mechanism emerging from these studies is a slightly more complex version of the previously proposed "dock-and-lock" mechanism (*23*), in which a rapid, reversible binding of monomer to the fibril is followed by two successive, relatively slow, steps in the SPR-based mechanism, versus a single ("locking") step in the dock-and-lock mechanism.

Gratifyingly, when the SPR microscopic rate constants are propagated by multiplication into a macroscopic equilibrium constant, the value obtained is 0.79 μM, well within the range of 0.7−1.0 μM for macroscopic fibril dissociation equilibrium constants (or C_rs) reported here. The SPR experiments were performed using the same Aβ(1−40) material, disaggregated and grown into fibrils using the same protocols used here. The PBS buffer was identical in both experiments. However, the Biacore analysis was conducted at 20 °C, while the experiments performed here were routinely done at 37 °C. However, we recently determined the C_r for Aβ(1−40) to be in the range of 1.2 μM at 19 °C (A. D. Williams, personal communication), which is therefore in very good agreement with the SPR result at 20 °C. Although the work described in this paper is primarily focused on fibril thermodynamics, the excellent agreement of the macroscopic C_r with the propagated microscopic rate constants generally supports dock-and-lock-type mechanisms and, in particular, demonstrates the ability to obtain details of the elongation reaction cycle through SPR studies with global fits of kinetic data (*22*).

Stability of Fibrils Grown in Thioflavin T. As a test of the utility of these C_r values in analyzing fibril structure and assembly, we ask whether the presence during elongation of a saturating concentration of the amyloid-binding dye ThT appreciably alters the stability of the fibril, in analogy to the ability of bound ligands to stabilize the folded states of globular proteins (see, for example, ref *24*). Although the

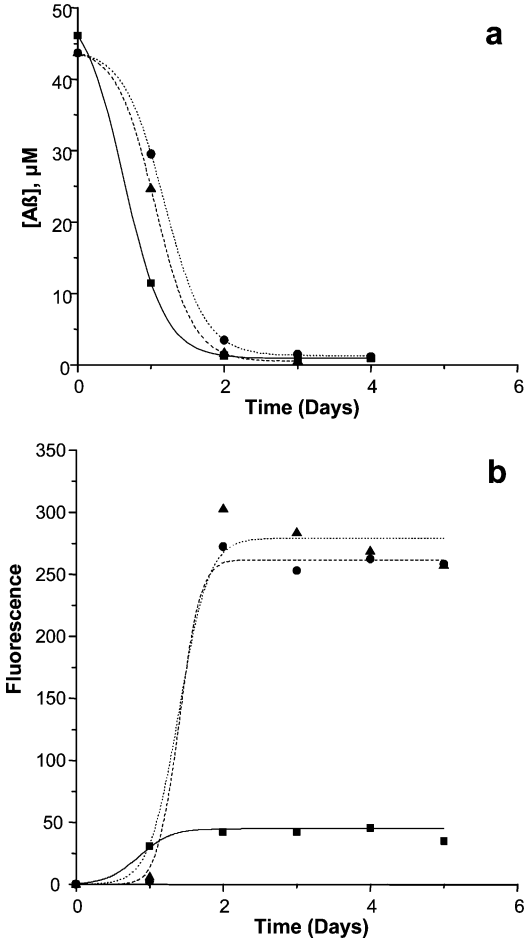

FIGURE 6: Aβ(1−40) fibril formation in the presence and absence of saturating amounts of ThT monitored by the HPLC sedimentation assay (a) and the standard ThT assay (b). 45 μM Aβ(1−40) was incubated alone (■) or in the presence of 45 μM (▲) or 90 μM (●) ThT. C_r values are listed in Table 1.

ThT assay as originally conceived and implemented involves the addition of fibrils to a test solution of thioflavin (*14*, *15*), more recently a modification has emerged in which fibrils are grown and monitored in the continuous presence of ThT (*25*). On the basis of the above logic of ligand stabilization, we were concerned that ThT binding to fibrils and intermediate structures might alter the course of reaction. Seeded Aβ(1−40) elongation reactions were initiated in the presence or absence of ThT and monitored by the HPLC sedimentation assay and by the standard ThT assay. The results are shown in Figure 6. Figure 6a shows that the presence of ThT in the reaction mixture modestly slows down fibril growth but that the reactions in the presence and absence of ThT reach very similar final equilibrium positions. The C_r values for WT and mutant fibrils grown in ThT are listed in Table 1. Interestingly, there is no detectable difference in the free energy of fibril elongation in the presence or absence of ThT. On one hand, this might be considered to be not unexpected, given the relatively low binding stoichiometry of ThT to Aβ fibrils; multiple binding sites have been reported recently (*26*, *27*), with binding constants below the 45−90 μM used in the experiments reported here and with binding stoichiometries ranging from 1:300 ThT molecules per Aβ molecule to 1:4 ThT per Aβ. On the other hand, since the free energies reported here specifically report on the elongation steps occurring on the fibril ends, one still might have expected an effect on apparent stability if one of the ThT binding sites corresponds to fibril growth termini [since fibrils contain hundreds to thousands of Aβ monomers per fibril, binding to fibril ends would give the reported (*26*, *27*) low ThT binding stoichiometry].

Figure 6b shows the time courses of the same reactions monitored by ThT. There are two dramatic effects. First, fibrils grown in the presence of ThT exhibit substantially higher fluorescence values than fibrils grown in the absence of ThT. This is not due to a change in fluorescence spectrum (data not shown). The additional fluorescence is also not associated with a second class of loosely bound ThT, since the high fluorescence yield survives buffer washes to remove any excess ThT (data not shown). The source of the increased signal is not clear. If ThT interacts with fibrils by being sequestered in an ordered array in the fibril interior, it is reasonable to conclude that fibrils grown in the presence of ThT might acquire a larger load of ThT. Alternatively, if the ThT effect is produced by binding to the growing ends of fibrils, a larger signal might arise if growth of fibrils in the presence of ThT led to shorter fibrils. However, this seems unlikely since (a) sonication of a fibril preparation does not produce large increases in ThT signal and (b) the lack of effect on the free energy of elongation suggests that binding sites are not on the fibril ends (see above).

The second interesting feature of the ThT-monitored kinetics is the day 1 values for the two reactions. On day 1, the elongation reaction run in the absence of ThT has gone over 50% to completion, as monitored both by ThT (Figure 6b) and by HPLC analysis (Figure 6a). In contrast, the ThT signal has progressed negligibly by day 1 for the reaction done in the presence of ThT, even though the reaction is nearly 50% complete by HPLC. The most likely explanation for this discrepancy is that the presence of ThT induces formation of an initial, ThT-negative aggregate, which eventually is channeled into amyloid fibril formation. One candidate for this alternative aggregate is the protofibril, which exhibits low ThT response (*28*, *29*). The formation of protofibrils in the +ThT reaction might be due to a positive effect of ThT inducing protofibril formation, as seen for other small molecules (*29*), or to inhibition of seeded fibril elongation, leading to competing formation of protofibrils from the high concentration of monomeric Aβ(1−40). This is consistent with the observation of the formation of protofibrils at day 1 in unseeded reactions conducted under these conditions (*29*). Further studies are required to confirm and better understand this possible inhibitory effect.

Analysis of Elongation Kinetic Data. The standard approach to analyzing amyloid elongation kinetic data from ThT measurements is to assume that the fluorescence when the reaction reaches a plateau reflects the conversion of all of the amyloidogenic peptide to amyloid. We addressed the question of whether it might not be better to adjust the final ThT fluorescence value to take into account the knowledge that the amyloid formation reaction is incomplete.

Figure 1b shows several variations of kinetic treatments of the data from Figure 1a. A standard pseudo-first-order treatment, for a reaction that essentially goes to completion, of the monomer concentration data from HPLC gives a rate constant of $-1.236\ h^{-1}$ (◆). However, since the finite critical concentration of Aβ(1−40) in these reactions makes it clear

that the reaction does not go to completion, we applied the standard treatment for reversible first-order kinetic data (*20*) (see Materials and Methods) to the HPLC data to obtain a rate for k_{obs} of -1.322 h^{-1} (■). The standard approach to plotting ThT fluorescence data, in which the fluorescence at plateau is considered to represent the complete conversion of monomer to fibrils, gives a rate of -1.378 h^{-1} (□). Finally, as a complement to the standard ThT treatment, we adjusted the final fluorescence value used in the kinetic treatment to reflect the amount of fluorescence one would obtain if all of the monomers were converted to fibrils (instead of stopping at equilibrium) by multiplying the plateau fluorescence value times the ratio $[M_{initial}]/([M_{initial}] - C_r)$. A first-order kinetic treatment of these data gives a rate constant of -1.202 h^{-1} (◇).

While the correction of the HPLC data (■) forces the kinetics to trend toward the equilibrium position, the correction of the ThT fluorescence data (◇) adjusts a reaction curve that inherently reflects the equilibrium position to the curve that would have been obtained were the reaction irreversible. As expected on the basis of the above discussion of the nature of the corrections for a finite C_r, the rate constants obtained from treatment of uncorrected HPLC data and corrected fluorescence data are in close agreement, while the rate constants obtained from treatment of corrected HPLC data and uncorrected ThT data are also in close agreement. Thus, although intuitively one might be inclined to adjust the ThT data for fibrils with significant C_r values, in fact it is preferable to use nonnormalized data, which is already internally normalized for the back-reaction.

DISCUSSION

The experiments described here show unequivocally that the residual peptide monomer remaining when an Aβ(1−40) fibril assembly reaction reaches a plateau is a true C_r value reflecting a point of dynamic equilibrium in fibril assembly. This material is chemically identical to the monomers that have incorporated into the fibril and is itself capable of forming fibrils. The same equilibrium position is attained when isolated Aβ(1−40) fibrils are allowed to dissociate. Furthermore, the average size or molecular weights of the fibril population, and hence the molar concentration of fibril growing ends, do not appreciably affect the final C_r value. Finally, the growth equilibrium constant calculated from the ratio of reverse and forward rate constants is in very good agreement with the value obtained from the critical concentration, C_r (Table 1), and with propagated microscopic rate constants from SPR studies (*22*).

Although prolonged incubation of an Aβ(1−40) fibril assembly reaction leads to further losses of monomer from solution and smaller values for the apparent C_r, we show here that this continual, gradual further stabilization of the fibrils seems to derive from a secondary physical change in the fibrils, such as clustering, that is reversed on sample handling. Thus, the C_r value of about 0.8 μM, corresponding to a ΔG for fibril formation of about -8.6 kcal/mol, appears to be a characteristic value representing the stability of the isolated Aβ(1−40) amyloid fibrils prepared as described here. It is possible that Aβ(1−40) fibrils prepared differently, such as with continuous agitation (*30*), might exhibit somewhat different stabilities; stability is apparently one aspect of fibril structure that can vary with different conformational states of fibrils made from the same peptide (*31*).

Our data suggest several practical lessons for obtaining similar C_r values in other amyloid systems. At least with Aβ(1−40), it is possible to derive C_r values by approaching equilibrium either in the elongation or in the dissociation direction. The potential advantage of using dissociation is that it should eliminate the possible effect of chemical derivatives of the amyloidogenic peptide, such as synthetic side products, that are incapable of being incorporated into fibrils. The disadvantage is that there may be cases in which a finite C_r exists but cannot be conveniently approached by fibril dissociation due to a kinetic barrier (A. M. Bhatacharyya and R. Wetzel, unpublished results). When approaching equilibrium via elongation, on the other hand, it appears to be important to arrange an aggressive elongation rate (by strong seeding), so that the C_r characteristic of well-behaved fibrils can be kinetically distinguished from lower values associated with secondary phenomena like that shown in Figure 1c.

The existence of apparent equilibrium positions for fibril formation by various Aβ-related peptides has been reported, implied, and/or discussed previously (*7*−*10*, *22*, *32*−*35*). Using radiolabeled Aβ peptides, the Lansbury group reported C_r values for Aβ(1−40) in the 5−10 μM range (*7*, *8*). It is possible that these values are higher than our C_r value because of the lower salt concentration in the buffer in their reactions; higher salt concentrations tend to enhance hydrophobic interactions (*36*), which are known to play a significant role in the stability of the Aβ(1−40) fibril (*37*). Using SPR to follow Aβ(1−40) fibril assembly, Hasagawa et al. reported C_r values of 0.02 and 0.2 μM, depending on the details of the measurement (*35*). The reason for the discrepancy of these values with the value of 0.8 μM reported here is not clear but may be due to differences in the peptide source, material handling protocols or buffers, and the reaction temperature or could be due to differences in SPR methodology and data analysis. Interestingly, we show here (Results) that microscopic rate constants from a global fit of SPR data obtained at different Aβ concentrations (*22*) yield a macroscopic equilibrium constant very close to the C_r values reported here (Table 1).

Most assessments of "amyloidogenicity" have been done at the level of fibril growth kinetics (*38*). Although kinetic analysis can give useful energetic information, the use of kinetics in most amyloid studies is made additionally complex by uncertainties about the mechanism (*39*, *40*). The kinetics of seeded elongation reactions, which can bypass uncertainties about mechanisms of reaction initiation, is a feasible alternative (*12*), but complete analysis and interpretation will depend on development of methods for estimating average fibril molecular weight (*18*). Compared to kinetic approaches, the thermodynamics of fibril elongation offers much more accessible data and cleaner, more direct interpretations that give values consistent with those obtained from studies on globular proteins (*37*). Ultimately, a full description of fibril formation will require information on both kinetics and thermodynamics.

We show here that saturation of the ThT binding site on the Aβ(1−40) fibril does not confer significant additional stability to the fibril. This somewhat surprising result has

implications for the nature of the ThT interaction with amyloid fibrils, a complex story involving multiple binding sites, none of which has been localized to the fibril structure (*26*, *27*). In a similar way it should now be possible to undertake systematic studies on the effect of variations in salt, pH, temperature, etc. on the energetics of amyloid fibril elongation, in analogy to classical studies on protein folding. Analysis of the energetic consequences of mutational effects on fibril stability, another classical approach to protein folding, can also be conducted using methods described here (*10*, *21*, *37*, *41*). Although analysis of Aβ fibril stability is simplified by an equilibrium position that is easily measured under native buffer conditions, it should also be possible to determine fibril stability for amyloid fibrils more stable than those of Aβ by using solvent denaturation (*42*) methods similar to those that are routinely applied to the analysis of the folding stability of globular proteins (*43*).

ACKNOWLEDGMENT

We gratefully acknowledge Elizabeth Howell for helpful discussions.

REFERENCES

1. Wetzel, R. (1994) Mutations and off-pathway aggregation, *Trends Biotechnol. 12*, 193−198.
2. Wetzel, R. (1997) Domain stability in immunoglobulin light chain deposition disorders, in *Protein Misassembly* (Wetzel, R., Ed.) pp 183−242, Academic Press, San Diego.
3. Selkoe, D. J. (1994) Normal and abnormal biology of the β-amyloid precursor protein, *Annu. Rev. Neurosci. 17*, 489−517.
4. De Young, L. R., Dill, K. A., and Fink, A. L. (1993) Aggregation and denaturation of apomyoglobin in aqueous urea solutions, *Biochemistry 32*, 3877−3886.
5. Clark, P. L. (2004) Protein folding in the cell: reshaping the folding funnel, *Trends Biochem. Sci. 29*, 527−534.
6. Matthews, B. W. (1993) Structural and genetic analysis of protein stability, *Annu. Rev. Biochem. 62*, 139−160.
7. Jarrett, J. T., Berger, E. P., and Lansbury, P. T., Jr. (1993) The carboxy terminus of the beta amyloid protein is critical for the seeding of amyloid formation: implications for the pathogenesis of Alzheimer's disease, *Biochemistry 32*, 4693−4697.
8. Jarrett, J. T., Costa, P. R., Griffin, R. G., and Lansbury, P. T., Jr. (1994) Models of the b protein C-terminus: differences in amyloid structure may lead to segregation of "long" and "short" fibrils, *J. Am. Chem. Soc. 116*, 9741−9742.
9. Harper, J. D., and Lansbury, P. T., Jr. (1997) Models of amyloid seeding in Alzheimer's disease and scrapie: mechanistic truths and physiological consequences of the time-dependent solubility of amyloid proteins, *Annu. Rev. Biochem. 66*, 385−407.
10. Williams, A. D., Portelius, E., Kheterpal, I., Guo, J. T., Cook, K. D., Xu, Y., and Wetzel, R. (2004) Mapping abeta amyloid fibril secondary structure using scanning proline mutagenesis, *J. Mol. Biol. 335*, 833−842.
11. Zagorski, M. G., Yang, J., Shao, H., Ma, K., Zeng, H., and Hong, A. (1999) Methodological and chemical factors affecting amyloid-β amyloidogenicity, *Methods Enzymol. 309*, 189−204.
12. O'Nuallain, B., Williams, A. D., Westermark, P., and Wetzel, R. (2004) Seeding specificity in amyloid growth induced by heterologous fibrils, *J. Biol. Chem. 279*, 17490−17499.
13. Kheterpal, I., Williams, A., Murphy, C., Bledsoe, B., and Wetzel, R. (2001) Structural features of the Aβ amyloid fibril elucidated by limited proteolysis, *Biochemistry 40*, 11757−11767.
14. Naiki, H., and Gejyo, F. (1999) Kinetic analysis of amyloid fibril formation, *Methods Enzymol. 309*, 305−318.
15. LeVine, H. (1999) Quantification of β-sheet amyloid fibril structures with thioflavin T, *Methods Enzymol. 309*, 274−284.
16. Kheterpal, I., Zhou, S., Cook, K. D., and Wetzel, R. (2000) Abeta amyloid fibrils possess a core structure highly resistant to hydrogen exchange, *Proc. Natl. Acad. Sci. U.S.A. 97*, 13597−13601.
17. Kheterpal, I., Wetzel, R., and Cook, K. (2003) Enhanced correction methods for hydrogen exchange-mass spectrometry studies of amyloid fibrils, *Protein Sci. 12*, 635−643.
18. Bhattacharyya, A. M., Thakur, A., and Wetzel, R. (2005) Polyglutamine aggregation nucleation: thermodynamics of a highly unfavorable protein folding reaction (submitted for publication).
19. Ferrone, F. (1999) Analysis of protein aggregation kinetics, *Methods Enzymol. 309*, 256−274.
20. Frost, A. A., and Pearson, R. G. (1961) *Kinetics and Mechanism*, 2nd ed., Wiley, New York.
21. Shivaprasad, S., and Wetzel, R. (2004) An intersheet packing interaction in Aβ fibrils mapped by disulfide cross-linking, *Biochemistry 43*, 15310−15317.
22. Cannon, M. J., Williams, A., Wetzel, R., and Myszka, D. G. (2004) Kinetic analysis of Aβ fibril elongation, *Anal. Biochem. 328*, 67−75.
23. Esler, W. P., Stimson, E. R., Jennings, J. M., Vinters, H. V., Ghilardi, J. R., Lee, J. P., Mantyh, P. W., and Maggio, J. E. (2000) Alzheimer's disease amyloid propagation by a template-dependent dock-lock mechanism, *Biochemistry 39*, 6288−6295.
24. Miroy, G. J., Lai, Z., Lashuel, H. A., Peterson, S. A., Strang, C., and Kelly, J. W. (1996) Inhibiting transthyretin amyloid fibril formation via protein stabilization, *Proc. Natl. Acad. Sci. U.S.A. 93*, 15051−15056.
25. Wall, J., Murphy, C. L., and Solomon, A. (1999) In vitro immunoglobulin light chain fibrillogenesis, *Methods Enzymol.*, 204−217.
26. LeVine, H., III (2005) Multiple ligand binding sites on Aβ(1−40) fibrils, *Amyloid 12*, 5−14.
27. Lockhart, A., Ye, L., Judd, D. B., Merritt, A. T., Lowe, P. N., Morgenstern, J. L., Hong, G., Gee, A. D., and Brown, J. (2005) Evidence for the presence of three distinct binding sites for the thioflavin T class of Alzheimer's disease PET imaging agents on beta-amyloid peptide fibrils, *J. Biol. Chem. 280*, 7677−7684.
28. Kirkitadze, M. D., Condron, M. M., and Teplow, D. B. (2001) Identification and characterization of key kinetic intermediates in amyloid beta-protein fibrillogenesis, *J. Mol. Biol. 312*, 1103−1119.
29. Williams, A. D., Sega, M., Chen, M., Kheterpal, I., Geva, M., Berthelier, V., Kaleta, D. T., Cook, K. D., and Wetzel, R. (2005) Structural properties of Aβ protofibrils stabilized by a small molecule, *Proc. Natl. Acad. Sci. U.S.A. 102*, 7115−7120.
30. Petkova, A. T., Leapman, R. D., Guo, Z., Yau, W. M., Mattson, M. P., and Tycko, R. (2005) Self-propagating, molecular-level polymorphism in Alzheimer's β-amyloid fibrils, *Science 307*, 262−265.
31. Tanaka, M., Chien, P., Naber, N., Cooke, R., and Weissman, J. S. (2004) Conformational variations in an infectious protein determine prion strain differences, *Nature 428*, 323−328.
32. Wood, S. J., Wetzel, R., Martin, J. D., and Hurle, M. R. (1995) Prolines and amyloidogenicity in fragments of the Alzheimer's peptide β/A4, *Biochemistry 34*, 724−730.
33. Huang, T. H., Fraser, P. E., and Chakrabartty, A. (1997) Fibrillogenesis of Alzheimer Abeta peptides studied by fluorescence energy transfer, *J. Mol. Biol. 269*, 214−224.
34. Myszka, D. G., Wood, S. J., and Biere, A. L. (1999) Analysis of fibril elongation using surface plasmon resonance biosensors, *Methods Enzymol. 309*, 386−402.
35. Hasegawa, K., Ono, K., Yamada, M., and Naiki, H. (2002) Kinetic modeling and determination of reaction constants of Alzheimer's beta-amyloid fibril extension and dissociation using surface plasmon resonance, *Biochemistry 41*, 13489−13498.
36. Creighton, T. E. (1984) *Proteins: Structures and Molecular Properties*, W. H. Freeman, New York.
37. Williams, A. D., Shivaprasad, S., and Wetzel, R. (2005) Alanine scanning mutagenesis of Aβ(1−40) amyloid fibril stability (submitted for publication).
38. Chiti, F., Stefani, M., Taddei, N., Ramponi, G., and Dobson, C. M. (2003) Rationalization of the effects of mutations on peptide and protein aggregation rates, *Nature 424*, 805−808.
39. Serio, T. R., Cashikar, A. G., Kowal, A. S., Sawicki, G. J., Moslehi, J. J., Serpell, L., Arnsdorf, M. F., and Lindquist, S. L. (2000) Nucleated conformational conversion and the replication of conformational information by a prion determinant, *Science 289*, 1317−1321.
40. Collins, S. R., Douglass, A., Vale, R. D., and Weissman, J. S. (2004) Mechanism of prion propagation: efficient amyloid growth

in the absence of oligomeric intermediates, *PLoS Biol. 2*, 1582−1590.
41. Shivaprasad, S., and Wetzel, R. (2005) Scanning cysteine mutagenesis analysis of Aβ(1−40) amyloid fibrils (submitted for publication).
42. Narimoto, T., Sakurai, K., Okamoto, A., Chatani, E., Hoshino, M., Hasegawa, K., Naiki, H., and Goto, Y. (2004) Conformational stability of amyloid fibrils of beta2-microglobulin probed by guanidine-hydrochloride-induced unfolding, *FEBS Lett. 576*, 313−319.
43. Pace, C. N., Shirley, B. A., and Thomson, J. A. (1990) Measuring the conformational stability of a protein, in *Protein Structure—a practical approach* (Creighton, T. E., Ed.) pp 311−330, IRL Press, Oxford, England.

BI050927H